

Shining a light on disease with MIR fibre-optics

Angela B. Seddon^{*a}, Bruce Napier^b, Ian Lindsay^c, Samir Lamrini^d, Peter M. Moselund^e, Nicholas Stone^f, Ole Bang^g and Mark Farries^h

^{a.} *MIR Photonics Group, George Green Institute for Electromagnetics' Research, Faculty of Engineering, University of Nottingham, NG7 2RD, UK.*

^{b.} *Vivid Components Ltd. German Office, Dr-Rörig-Damm 22, 33102 Paderborn, Germany.*

^{c.} *Gooch & Housego, UK, now at H. H. Wills Physics Laboratory, Tyndall Ave., University of Bristol, BS8 1TL, UK.*

^{d.} *LISA laser products OHG, Fuhrberg & Teichmann, Albert Einstein Straße, 1-9 37191 Katlenburg-Lindau, Germany.*

^{e.} *NKT Photonics A/S, Blokken 84 - DK-3460 Birkerød, Denmark.*

^{f.} *Physics and Astronomy, College of Engineering, Mathematics and Physical Sciences, University of Exeter, EX4 4QL, UK.*

^{g.} *Fibre Sensors and Supercontinuum Group, DTU Fotonik, Technical University of Denmark, DK-2800 Kongens Lyngby, Denmark.*

^{h.} *Gooch & Housego, Broomhill Way, Torquay, TQ2 7QL, UK.*

ABSTRACT – TO BE WRITTEN

Introduction

MINERVA Project aims

This article highlights the role that mid-infrared (MIR) fibre-optics may play in *in vivo* diagnosis of disease, including cancer. We summarise here key results from the European funded FP7 Project: acronym: MINERVA, titled: " **M**id- to **NE**ar infrared spectroscopy for improv**E**d medical di**A**gnostics ", (Grant agreement no.: 317803, <http://minerva-project.eu/>) which ran 2012 to 2017. This article is based on our recent paper at SPEC2018 (June 2018; Chair: Dr Matthew J. Baker, University of Strathclyde, Glasgow, Scotland) in the 'Emerging Technologies' session.

Prior to MINERVA, it had already become clear that mid-infrared (MIR) imaging spectroscopy has the potential to open a new chapter in bio-medical imaging. MIR imaging spectroscopy offers an effective tool for early cancer diagnosis and improved survival rates. Great progress had been made by analysing the entire bio-molecular MIR spectral signature using automated statistical algorithms. However, the lack of suitable sources, detectors and components in 2012 appeared to restrict the technology to one of academic interest, based on weak thermal sources, low power lasers or synchrotron research tools.

MINERVA recognised that for the first time the photonic technology was in place to develop a new MIR technology platform based on MIR fibreoptics in which entirely novel supercontinuum (SC) fibre laser sources (at least 1000 x brighter than conventional blackbody sources like the Globalar[®]) that are

broadband would be developed, covering the MIR spectral region of interest for analysing cells, tissue and body fluids [1].

Two specific high impact applications were addressed in MINERVA: (i) high volume pathology screening *i.e.* automated microscope-based examination of cell and tissue excised biopsy samples, and (ii) *in vivo*, real-time skin surface examination *i.e.* non-invasive investigation of suspected skin cancer, working towards the MIR optical biopsy.

In this article we firstly set out the background to the MINERVA Project covering the current 'Gold Standard' for disease diagnosis and the current mid-infrared microspectroscopy approach to disease diagnosis. We then set out the MINERVA approach of a MIR fibreoptic system which aims in future to achieve MIR spectroscopy *in vivo* and the MIR optical biopsy. An overview of MIR glass fibreoptics is given. At the heart of the MIR fibreoptic system is the broadband fibre MIR-SC source, and its development in MINERVA, and beyond, is described. Finally, the first MIR imaging *ex vivo* using MIR fibreoptics and fibre MIR-SC laser sources is presented.

Background to the MINERVA Project

The current 'Gold Standard' of disease screening and diagnosis

Today, the 'Gold Standard' for identification of disease, including cancer, remains histopathology, that is: the visible-light microscopic study of the morphology of dye-stained cells and tissue to find out about disease. Histopathology is labour-intensive and highly dependent on the judgement of the pathologist. Major hospitals house a 'Path. Lab' where cells are taken, or biopsies of tissue excised from patients may be frozen, microtomed into slices of < 10 μm thickness that are individually mounted in sequential order on microscope slides, and stained with haematoxylin and eosin (H&E) dyes. Such dye-staining reveals the cell and tissue morphology for examination by the pathologist using optical microscopy to inform diagnosis and treatment planning. Patients usually must await their pathology results which leads to patient discomfort and healthcare costs. For instance, awaiting a pathology result of whether or not a tumour has been totally excised, where excised tumour margins are interrogated for malignancy, interrupts surgery, again with associated patient discomfort and healthcare costs.

Current mid-infrared (MIR) biomedical spectroscopy for disease screening and diagnosis

The biomedical spectroscopist Max Diem was the first to recognise that the MIR spectroscopic information revealed by cells and tissue may revolutionise the way that pathology is performed in the 21st Century [2]. Diem was in the vanguard of applying *in vitro* and *ex vivo* MIR spectroscopy of human cells and tissue. The important early contribution of Henry H. Mansch must also be recognised [3,4]. Diem's seminal paper [2] of 1999 was critical of some of the work prior to 1996, as being too simplistic about the use of MIR spectroscopy to detect malignant, as opposed to normal, cells and tissue because a 'cancer spectral peak' was sometimes assumed rather than subtle changes across the MIR spectral region. Diem highlighted that MIR spectroscopy of cells and tissue could potentially provide an immense amount of information on cellular composition, packing of cellular components, organ and cell architecture, metabolic processes and the absence/presence of disease. Analysing cell and tissue biopses *ex vivo* using MIR spectroscopy allows preservation of the anatomical arrangement of tissue enabling evaluation of the pathological features and histological architecture of tissue taken from patients. MIR spectral data processing utilises mathematical procedures (such as unsupervised principal component analysis) to analyse subtle spectral differences of the entire spectrum and it has been demonstrated that subtle differences do exist and that normal and diseased areas of tissue can be distinguished spectroscopically [2]. This type of automated pattern recognition of the families of vibrational absorption bands in the MIR spectra has formed the bedrock of advances in the field and may aid clinicians (medical professionals interacting directly with patients) in future in objective diagnosis. The field is expanding and consolidating. Biomedical MIR molecular vibrational absorption spectroscopy analysis of excised (cut-out) tissue and exfoliated cells is accruing evidence of the ability to distinguish diseased cells and tissue from normal cells and tissue (e.g. [5-9]). A Nature Protocol for sample treatment and measurement methodology has been written by 21 eminent authors in the field of biomedical MIR spectroscopy [10]. In addition, a 'barcode' approach has become popular [11], that is the reduction of full MIR spectral acquisition to some key spectral areas of difference between diseased and benign tissue and cells and this has allowed more effective numerical manipulation of the vast MIR spectral data sets. Nevertheless, it is important to realise that access to the whole MIR spectrum, if possible 3 to 15 μm wavelength is probably required in order to have enough specificity and sensitivity for objective disease diagnosis.

MIR microspectroscopy imaging is widely recognised as non-destructive, label-free, highly sensitive and is applied particularly in cancer research and diagnosis, *ex vivo* on excised tissue. State-of-the-art MIR imaging microspectroscopy was carried out during the MINERVA Project. Fig. 1 shows MIR microspectroscopic imaging of excised colon tissue carried out using a standard FTIR (Fourier

transform infrared) spectrometer with a weak, blackbody source (GloBar[®]) and mercury-cadmium telluride focal-plane-array (MCT-FPA) detection [12]. In achieving the 1 μm resolution MIR imaging, shown in Fig. 1, the Abbe diffraction limit of MIR radiation ($\sim 5 \mu\text{m}$) was overcome and this was accomplished by over-sampling.

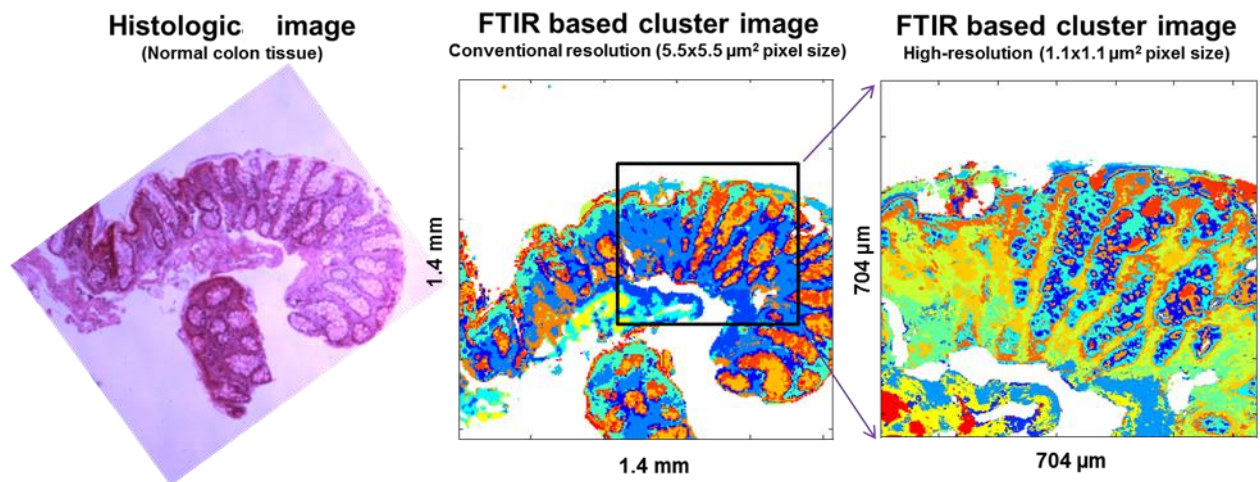


Figure 1. State-of-the-art MIR spectral images of excised normal colon tissue compared to a conventional histopathological micrograph of the H&E (*i.e.* haematoxylin and eosin) dye-stained colon tissue. In achieving the 1 μm resolution MIR imaging, the Abbe diffraction limit of MIR radiation ($\sim 5 \mu\text{m}$) was overcome and this was accomplished by over-sampling. (Images from the Group of N. Stone, University of Exeter, UK, Co-Investigator EU MINERVA [\(more in \[12\].\)](#))

In other MINERVA work numerical removal of paraffin from the MIR microspectroscopy of tissue which had been dried and paraffin impregnated was investigated [13].

Microspectroscopy for MIR spectral collection of cells and tissue utilises a desk-top instrument combining MIR microscopy with FTIR spectrometry. A typical laboratory set-up for MIR spectroscopic analysis is shown in Fig. 2. The traditional type of broadband MIR source is a blackbody, incandescent source with 3-dimensional emission, for instance from a SiC ceramic bar of a few mm dimensions, and is of low power. This has necessarily restricted that the optical circuit of source / analyte / detector be in close proximity in order to have enough photons available for detection.

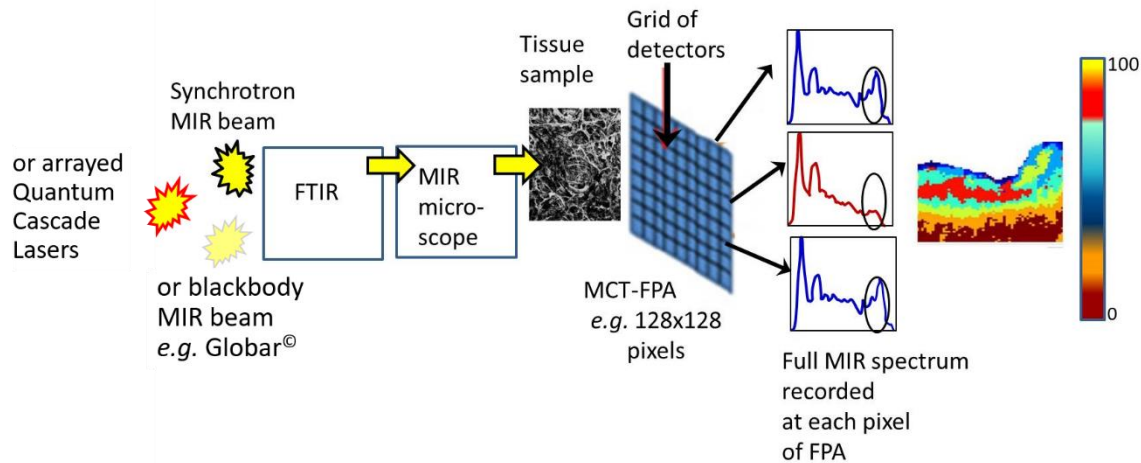


Figure 2. Traditional MIR spectral imaging of excised biological tissue involves a benchtop setup comprising a source beam (MIR blackbody or a synchrotron-generated MIR beam or, latterly, arrayed QCLs) which is passed through a FT-MIR spectrometer and onto the tissue sample in a MIR microscope. A MCT-FPA detector captures spectral images and records a full spectrum at each pixel. The acquired spectral sets are treated statistically to yield molecular discrimination across the MIR tissue image shown as a false colour map. The false colour map is obtained by establishing similarities in spectral patterns (mathematically), then grouping spectra accordingly, and finally assigning colour codes to form an objective map-free from subjective assignment. (Redrawn from [14].)

Synchrotron (SR) generated MIR light has also been utilised for MIR microspectral imaging. The MIR-SR light is a small aperture beam up to 1000 x brighter than the traditional blackbody source. To date the optical circuits used in conjunction with SR-generated MIR radiation have mimicked those used with the traditional weak blackbody sources. The recent advent of bright MIR QCLs (quantum cascade lasers) and ICLs (inter-band cascade lasers) has seen them integrated within the same type of optical circuit comprising a closely positioned source / analyte / detector.

To date MIR spectroscopic molecular mapping and imaging has been of excised biological tissue. In the future, with the help of chalcogenide-glass fibreoptics the MIR spectral region may be opened up for real-time, *in vivo* medical diagnostics [1, 14], enabling the MIR optical biopsy (*'opsy'* look at, *bio* the biology) for early diagnosis of external cancers, intra-operative detection of cancer-margins and the possibility of MIR endoscopy for early diagnosis of internal cancers and their precise removal. This was the approach that was developed within the MINERVA research.

Progress towards a MIR fibreoptic system for *in vivo* MIR spectroscopic imaging of tissue and the MIR optical biopsy

Proposed bench-top set-up

Fig. 3 shows one of the proposed bench-top set-ups whereby active and passive MIR fibreoptics may be used in future to collect cell and tissue MIR spectra *in situ* in the body. For instance, to act as a

fiberoptic probe for dermatological screening and early diagnosis of skin cancer where objective cancer screening might be carried out in primary care by the practice nurse. On the other hand, analogous to current endoscopes which work in the visible spectrum and give topological imaging of tissue *in vivo*, so MIR glass endoscopes may be developed to give chemical mapping and imaging of deep tissue *in vivo*. For instance MIR endoscopic spectroscopic imaging such as inside the gastric tract and gynaecologically for cancer screening, early cancer diagnosis and for intra-operative assistance to map cancer-margins to assist the surgeon.

The key advantages of an all-fibre set-up (Fig. 3) for MIR spectroscopic disease detection, as opposed to the more conventional system design (Fig. 2) are that MIR fibreoptics can provide:

- (i) bright, spatially coherent, diffraction-limited beams of excellent beam quality;
- (ii) potential remote sensing and imaging of diseased tissue *in vivo*, in real-time, and
- (iii) portable and compact all-fibre systems.

The set up shown in Fig. 3 requires development of three types of MIR optical fibre, each of which was addressed in MINERVA, viz.: (a) nonlinear MIR optical fibre for supercontinuum generation to provide the bright broadband MIR light; (b) rare earth ion doped narrow-band MIR fibre lasers capable of being pulsed that are required to pump the nonlinear fibre MIR-SC broadband laser light and (c) low optical loss passive fibre to route the MIR light to where it is needed.

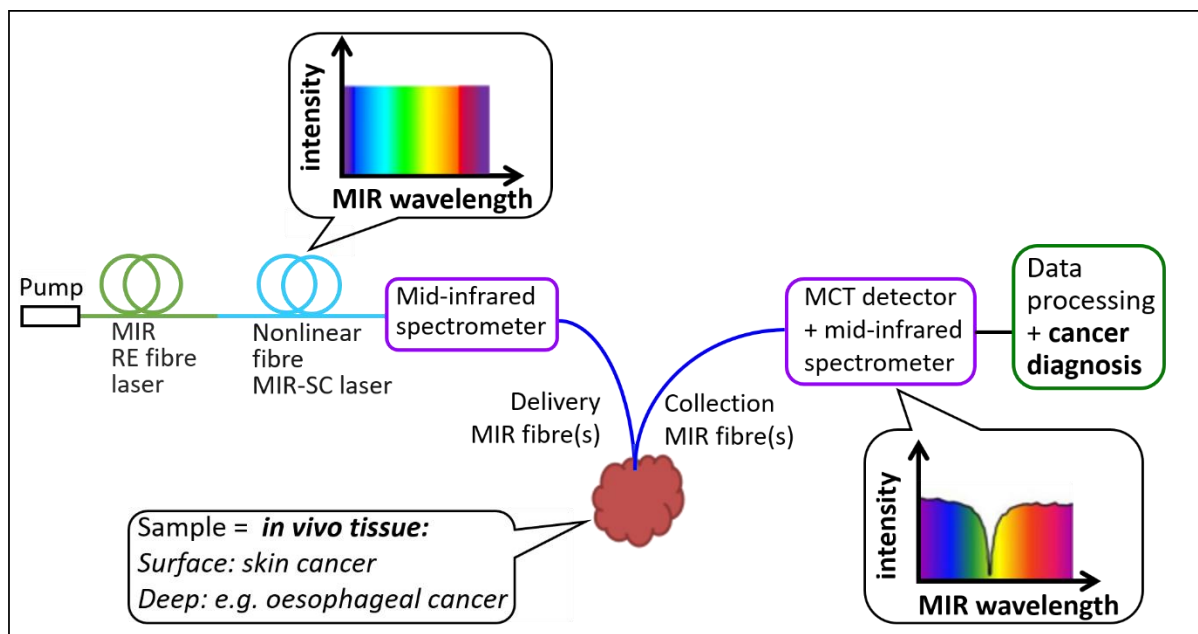


Figure 3. A proposed benchtop setup based on MIR fibreoptics to enable system-compactness, good beam quality and brightness with potential for *in vivo* detection of disease . The set-up comprises a MIR-SC (supercontinuum) fibre laser source (based on a nonlinear chalcogenide glass fibre) to provide bright broadband light which is spatially coherent. This is ideally achieved by pumping an optically nonlinear MIR glass fibre with a narrow-band MIR fibre laser $\geq 4.5 \mu\text{m}$

wavelength (based on a RE (rare earth ion doped) MIR glass fibre for direct emission) operating in the pulsed regime. The RE MIR fibre laser is in turn pumped with a commercial source. The fibre generated MIR-SC broadband light is passed through an optimised FT-MIR spectrometer and onto a patient's lesion *via* chalcogenide-glass passive MIR optical fibre or *via* a coherent bundle of MIR-transmitting optical fibres. Similarly, passive MIR fibre(s) collects the MIR light after tissue interaction and takes the MIR light to the detector. The spectral sets acquired from the light-tissue interaction are treated statistically to yield molecular discrimination and *in vivo* cancer diagnosis.

What is now required is FTIR spectrometers to be custom-made to accommodate small spatially coherent MIR optical beams, as opposed to the beam expansion demanded by current FTIR designs, whilst maintaining compatibility of the period of the FTIR interferometer with the pulse period of the fibre MIR-SC laser beam.

An alternative to FTIR, which was also addressed in MINERVA, is to use fibre MIR-SC lasers with fast MIR acousto-optic (A-O) filtering to select wavelengths of interest for detection. Within MINERVA, tellurite crystal A-O filtering was applied to the SWIR (short wave infrared (0.8 – 2.9 μm wavelength) and MWIR (mid-wave infrared: 3-5 μm wavelength); record large calomel crystals: Hg_2I_2 mercury (I) iodide were developed during the MINERVA Project for the LWIR region (long-wave infrared: 8-12 μm wavelength) out to at least 10 μm wavelength but the material longevity and properties were challenging.

Overview of MIR glass fibreoptics

The US National Research Council defines glass as: '*An X-ray amorphous solid which exhibits the glass transition (T_g), the latter being defined as that phenomenon in which a solid amorphous phase exhibits with changing temperature a more or less sudden change in the derivative thermodynamic properties such as heat capacity and expansion coefficient from crystal-like values to liquid-like values.*'

Note that: glass is a state of matter rather than a particular material; the glassy state can be formed by fast-cooling of a liquid to prevent atomic ordering (like crystallisation) and glasses only exist $< T_g$. **Fig. 4** is a plot of volume *per* unit mass *versus* temperature encompassing these ideas and showing glass is metastable with respect to the true equilibrium state - the crystalline state(s). From **Fig. 4**, shaping of glasses is carried out in the supercooled liquid regime ($T_g < \text{temperature} < T_m$) during melt-cooling or glass-reheating to above T_g . From **Fig. 4**, the beauty of glasses is the ability to form long fibre, by shaping in the supercooled liquid regime, for routeing light to where it is needed.

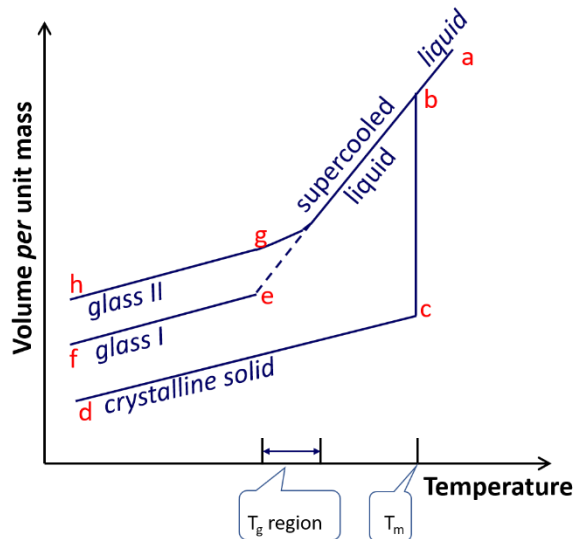


Figure 4. Phase behaviour of glasses. T_g is the glass transition temperature range and T_m is the liquidus. Path $abcd$ is a liquid freezing at the liquidus to a crystalline solid. For paths $abef$ or $abgh$, quenching is fast enough to prevent ordering on the atomic scale and the melt supercools. In the supercooled liquid regime, melt-shaping such as to form fibre can be carried out, at the appropriate melt viscosity, either during melt-quenching, or glass reheating, followed by cooling to ambient. Chalcogenide-glasses are formulated to avoid crystallisation of the supercooled liquid, which is thermodynamically driven but kinetically limited; so it is wise to limit the time spent in shaping. Glasses of different density (and hence different refractive index dispersion) are formed, depending on cooling-rate through the T_g range.

The University of Nottingham has pioneered extrusion of chalcogenide-glass melts to form (shape) fibreoptic preform rods and tubes and co-extruded fibreoptic preforms comprising a core glass rod concentrically surrounded by a lower refractive index optical cladding glass tube. Fibreoptic preforms are drawn down to fibre retaining the geometric shaping *pro rata* of the preform due to surface tension of the supercooled liquid during drawing. Light is confined in fibre due to total internal reflection within the higher refractive index core glass, and protected from evanescent field leakage by the lower index optical cladding glass, in so-called 'step-index fibres' (SIF). The numerical aperture (solid angle of acceptance of light in the fibre) depends only on the difference in refractive index of the core glass and surrounding cladding glass and hence the fibre can be very small diameter. At the University of Nottingham we make fibre core diameters from $4 \pm 1 \mu\text{m}$ to $300 \pm 5 \mu\text{m}$.

Chalcogenide glasses are a recognised group of inorganic glassy materials which are based on one or more chalcogen elements (Group XVI of Periodic Table): S, Se or Te, but not O, in conjunction with more electropositive elements to build robust glass matrices [15]. Both heteropolar (e.g., Ge-S) and homopolar (e.g., S-S; Ge-Ge) bonds can form. Thus glass formulations can contain a non-stoichiometric amount of chalcogen and excess S and Se atoms can form chains *etc.* The chemical bonding of the matrix is usually directional and covalent.

GeS₂, GeSe₂ and GeTe₂ glasses, for instance, are each isoelectronic with silicon dioxide glass - the basis of most common windows and container glasses - but consist of heavier atoms, more weakly bonded, thus according to the Szigetti equation [16]:

$$\nu \propto (f/m)^{1/2} \quad \text{eqn. 1}$$

(where: m is the reduced mass ($m = m_1m_2/(m_1+m_2)$) of the two vibrating atomic masses: m_1, m_2 ; f is the bond force constant which is related to the strength of the molecular bond) the vibrational absorption of chalcogenide-glasses is at smaller frequencies, ν (i.e. longer wavelengths) and hence they exhibit MIR transparency (see Fig.5). The heavy metal fluoride glass family (e.g. ZBLAN: ZrF₄-BaF₂-LaF₃-AlF₃-NaF) exhibit intermediate MIR transparency.

According to the International Standard: BSI ISO 20473:2007 [17], the MIR (mid-infrared) spectral region is defined as the 3-50 μm wavelength range. On the other hand, the DTGS (deuterated triglycine sulfate) detector, which is the most common room-temperature MIR detector, falls off in sensitivity at $\sim 25 \mu\text{m}$. Thus, often MIR spectroscopy spans 3-25 μm , which does cover most of the fundamental MIR vibrational absorption bands of biomolecular species. One important exception is that water exhibits fundamental vibrational absorption just below 3 μm wavelength (at ~ 2.7 and 2.9 μm , in the NIR (near-infrared) range [14]). The chalcogenide glasses according to Fig. 5 show a good overlap of transparency mapping onto the MIR spectra of biomolecules.

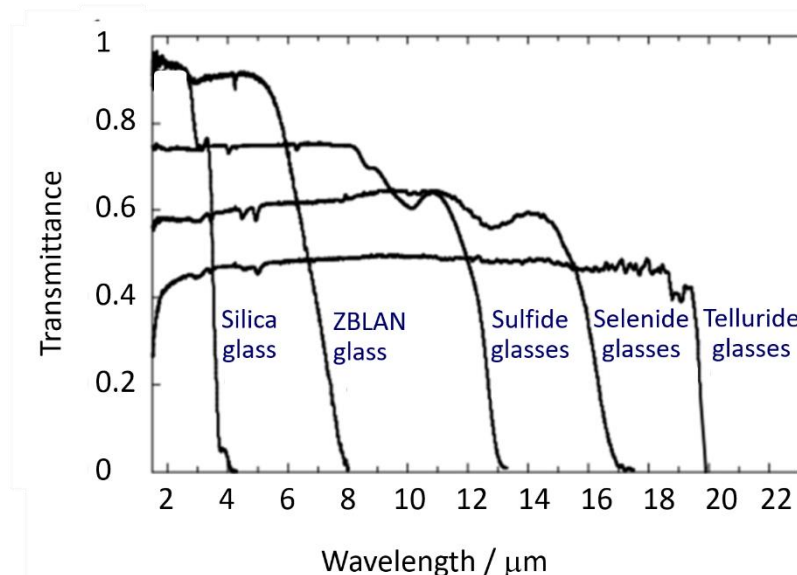


Figure 5. Relative transmittance of bulk glasses (of optical path length a few mm) based on silica-glass, a heavy metal fluoride glass (ZBLAN) and the chalcogenide-glasses: sulfides, selenides and tellurides showing the multiphonon cut-off edges moving to longer wavelength depending on the Szigetti equation (see text). Note that the baseline is dependent on

Fresnel reflection loss, in turn dependent on refractive index dispersion, at both incident and exit surfaces of the sample (Redrawn from [18].)

Progress in fibre mid-infrared supercontinuum generated broadband laser sources

From Fig. 3, at the heart of the MIR fibroptic approach to MIR tissue spectroscopy is the fibre MIR-SC broadband laser sources.

Supercontinuum (SC) generation was first reported by Alfano and Shapiro [19] in bulk silicate glasses. SC generation is a process whereby laser light is converted to light of broad spectral bandwidth with usually low temporal coherence and high spatial coherence. The spectral broadening is normally achieved by propagating short, high power, monochromatic optical pulses through an optically nonlinear medium at the zero dispersion wavelength.

St. J. Russell [20] reviewed SC generation in silica-glass-based photonic crystal fibre (PCF). Silica glass fibre visible (VIS) and near-infrared (NIR) broadband supercontinuum lasers are commercially available and can exceed by 10^6 x the brightness of similar wavelength range incandescent sources (Fig. 7). The physical processes behind fibre SC generation depend on pump pulse duration, peak power and repetition rate, pump wavelength, fibre chromatic dispersion and usually fibre length. For fs pump pulses, spectral broadening can be dominantly caused by self-phase modulation. In the anomalous dispersion regime, the combination of self-phase modulation and dispersion can lead to complicated soliton dynamics, including the splitting-up of higher-order solitons into multiple fundamental solitons (*soliton fission*). On pumping SC with ps, ns pulses, or even with CW (continuous wave) multi-Watt radiation, then Raman scattering and four-wave mixing can be important.

Fibre MIR-SC sources for the MWIR (mid-wave infrared) 3-5 μm wavelength range have become commercially available in the last 3 years. Silica glass is opaque in the MIR spectral region and so these commercial sources have been mainly based on heavy metal fluoride glasses (see Fig. 5).

MIR-transparent chalcogenide glasses are based on S, Se and Te atoms which have large, polarisable electron clouds, manifesting large linear refractive indices of the chalcogenide glasses and high nonlinear refractive indices [21] promising short fibre, and waveguide, MIR-SC generation devices.

Fig. 6 shows an early result in pumping a chalcogenide sulfide glass optical fibre with a fibre seed laser of wavelength 2.5 μm . The MIR-SC was curtailed at $\sim 5 \mu\text{m}$ wavelength [see Table 1] due, the Authors said, to the innate multiphonon edge absorption of the sulfide-based glass fibre used [22]. The importance of this result was to demonstrate MIR-SC in an *all-solid* optical fibre, of modest numerical aperture, rather than a photonic crystal fibre or fibre taper – so-called ‘holey’ fibres. It is a great advantage to be able to use a standard core / cladding, step-index fibre in the chalcogenide glasses because: (i) the mechanical fracture stress of the chalcogenides is about 1/5 that of silica glass fibres [23] and (ii) their Vicker’s Hardness is about 2 GPa compared to that of a standard soda-lime-silica glass of 5.5 GPa [24]. Thus, ‘holey’ chalcogenide glass fibre is: (I) vulnerable to fracture of the inner thin glass walls and (II) there is evidence, that sulfide-chalcogenide glass photonic crystal fibres deteriorate with time, suffering increasing optical loss, under exposure to ambient humidity and oxygen, perhaps due to the high glass surface area inside the propagating medium [25].

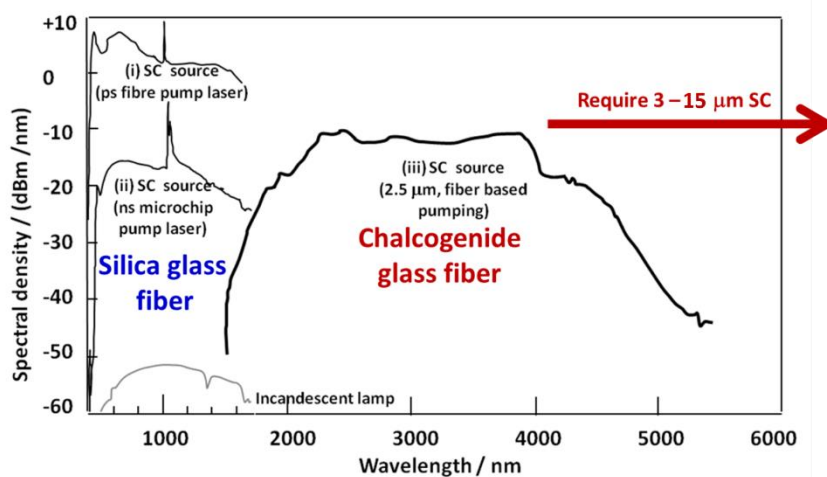


Figure 6. Supercontinuum (SC) generated broadband light across the near-infrared (NIR) and MIR spectral regions, reported prior to MINERVA, replotted here for comparison of brightness and output spectral range of various broadband light sources. Plots (i) and (ii) are based on silica-glass fibre in the visible (VIS) and NIR spectral regions and are adapted from [20]. Plot (iii) is based on chalcogenide glass fibre in the MIR spectral region and adapted from [22]. The incandescent lamp plot is adapted from [20]. MIR SCG spanning 3 to ideally 15 μm is required in order to be of use in collecting MIR spectra of biomolecular samples – as indicated by the horizontal arrow. (Redrawn from [1].)

However, as already shown in Fig. 6, a spectrally-bright fibre MIR-SC covering the whole span of 3 to at least 10 μm , preferably out to 15 μm wavelength, is required for collecting informative MIR spectra of biomolecular samples in order to have sufficient sensitivity and specificity of the MIR biomolecular sensing. The idea was first mooted in 2011 [1] to pump at a longer wavelength in a lower phonon energy chalcogenide glass fibre than in [22] (in Fig. 6) in order to try to generate a MIR-SC of ideal span for application in wideband MIR spectral imaging of biomolecular samples. In 2013, numerical modelling, led by O. Bang of DTU (Denmark) in the MINERVA Project, for the first time showed the feasibility of generating a 3- \geq 12 μm MIR-SC in chalcogenide glass fibre to span the MIR absorption bands of biomolecules [26]. The modelling was based on the measured refractive index dispersion [27] of two chalcogenide-glasses already developed as a matched glass-pair for co-processing, with very disparate refractive indices and so as to form a very high numerical aperture step-index fibre (SIF), with zero dispersion at just less than 8 μm for small core diameters.

The modelling assumed that the chalcogenide-glass fibre MIR-SC was pumped with a mode-locked, rare earth ion doped chalcogenide-glass fibre laser with emission at 4.5 μm wavelength (not yet experimentally developed – see next sub-section), with repetition rate 4 MHz, 50 ps long pulses and peak power 4.7 kW. Fibres of 8 and 10 μm core diameters in the numerical modelling generated a MIR-SC out to 12.5 and 10.7 μm , respectively, in less than 2 m of fibre when pumped with 0.75 and 1 kW, respectively, and the power converted into the 8-10 μm wavelength band was 7.5 and 8.8 mW, respectively.

A major achievement in MINERVA was chalcogenide-glass fibre MIR-SC was from 1.4 μm to 13.3 μm spectral range in fibre [28]. This was the first experimental demonstration truly to reveal the potential of MIR fibres to emit across the MIR molecular "fingerprint region" and a key first step towards portable, broadband MIR sources for real-time MIR molecular sensing [28, 29] (Fig. 7). In detail: it was demonstrated experimentally that launching intense, ultra-short fs pulses, with a central wavelength of either 4.5 μm , or 6.3 μm , into short pieces of ultra-high numerical-aperture, chalcogenide-glass SIF generated record MIR-SC, spanning 1.5 μm to 11.7 μm , and 1.4 μm to 13.3 μm , respectively (see Fig. 7(A) and (B) and Table 1). Output MIR-SCG power, for fs pumping of the fibre at a few pW average power, was a few 100s μW . Seeding of the fibre record MIR SC was with a non-collinear and difference frequency generation unit pumped by an optical parametric amplifier. The dip in the MIR-SC power out at \sim 11.5-12.5 μm wavelength in Fig. 7 was due to extrinsic

absorption loss arising from oxide contamination in the chalcogenide-glass fibre. These glass fibres were not ultra-purified and the MIR-SC output power, particularly at $\sim 12 \mu\text{m}$ wavelength, therefore has a possibility of further improvement.

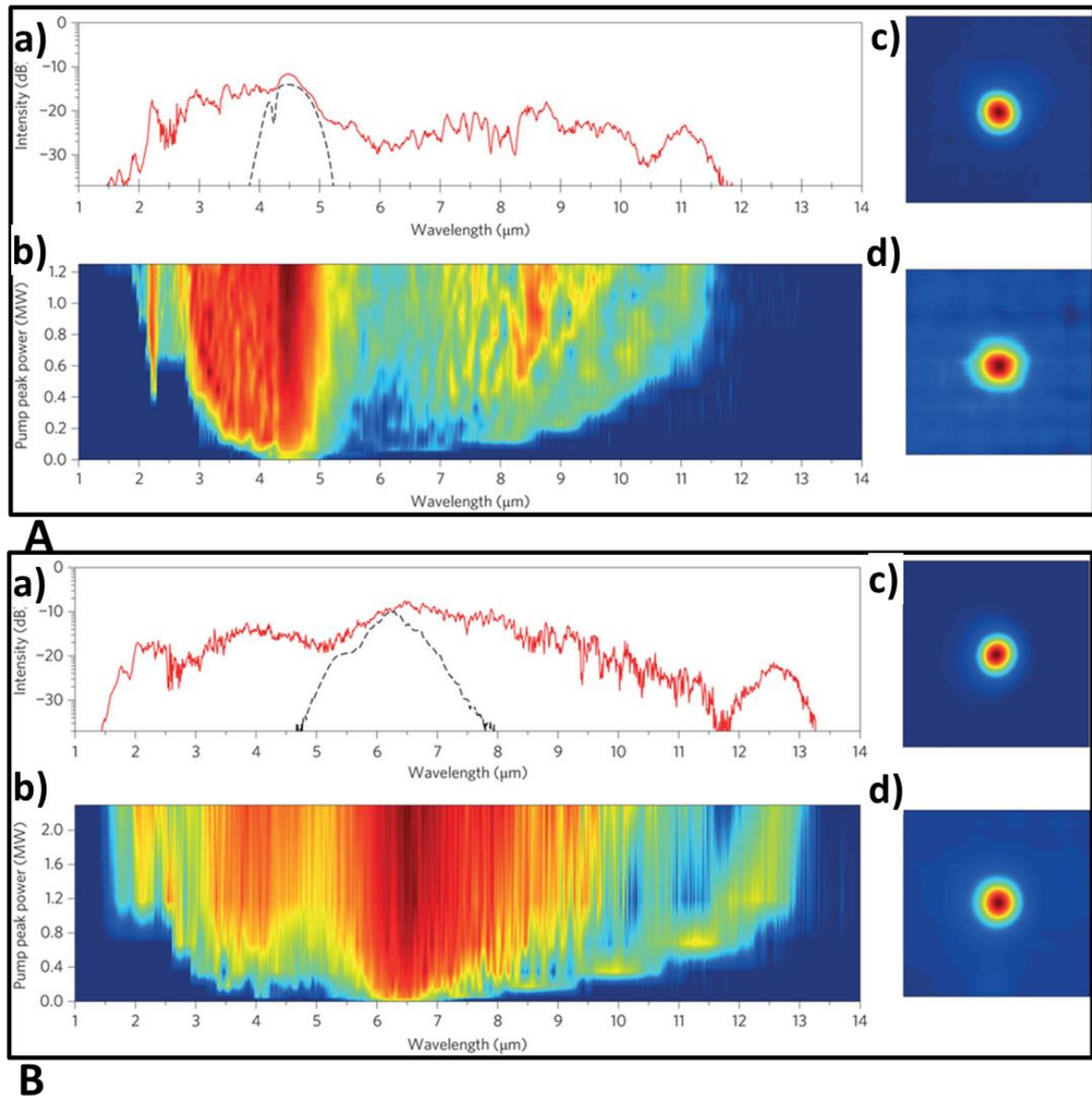


Figure 7. Details of record MIR-SC (MIR supercontinuum) generation [28]:

A a) Input pump spectrum (dashed line) and spectral profile at maximum pump power (solid line), showing relatively flat NIR- and MIR-SC ($2.08\text{--}10.29 \mu\text{m}$ @ -20 dB from signal peak) with distinct soliton peaks $> \text{ZDW}$ (zero dispersion wavelength) of $\sim 5.83 \mu\text{m}$, especially at $11 \mu\text{m}$. **b)** Spectral evolution with increasing pump peak power, showing gradual redshift of distinct soliton peaks $> \text{ZDW}$, and a combination of SPM (self-phase modulation) and dispersive waves $<$ the pump wavelength. **c), d)** Fibre output near-field beam profile corresponding to the spectrum in **a)** for all wavelengths **c)** and beam profile for wavelengths $> 7.3 \mu\text{m}$ only **d)**, showing that long wavelengths are still confined to the core.

B a) Input pump spectrum (dashed line) and spectral profile at maximum pump power (solid line), showing a broad, flat NIR- and MIR-SC ($1.64\text{--}11.38 \mu\text{m}$ @ -20 dB) followed by a strong spectral peak extending the spectrum all the way to $13.3 \mu\text{m}$. **b)** Spectral evolution with increasing pump peak power, showing gradual red-shift of a distinct spectral peak at the

long-wavelength edge and corresponding formation and blue-shift of dispersive waves. **c), d)** Fibre output near-field beam profile corresponding to spectrum in a) for all wavelengths **c)** and beam profile for wavelengths $>7.3 \mu\text{m}$ only **d)**, showing that long wavelengths are still confined to the core. (Image courtesy of [28].)

As pointed out in [30], an important practical factor is that the power required to generate the MIR-SC should be relatively low (a few kW) and compact, high-repetition-rate, pump sources with 10s or 100s mW of average power should instead be employed. Thus pumping a 110 mm high NA chalcogenide SIF with a relatively low peak pulse power of $\sim 3 \text{ kW}$ and 330 fs duration pulses, was shown to give rise to a MIR-SC spanning ~ 1.8 to $10 \mu\text{m}$ (Table 1). The pump was a customised fs OPA (*optical parametric amplifier*). Importantly, this allowed a MIR-SC of a few mW average power to be generated, as the Authors stated: "similar to that of a typical MIR beamline of a synchrotron". More recently, the group of Luther-Davies has achieved a fibre MIR-SC spanning 2.2 - $12 \mu\text{m}$ with 17 mW average power output [31]. Table 1 summarises the performance of some of the widest-band all-solid, step-index fibre MIR-SC lasers reported to date, with details of average output power and pump arrangement, together with a tapered chalcogenide -glass photonic crystal fibre for comparison [32].

Table 1. Chalcogenide-glass MIR-SC fibre lasers reported to date, arranged \leftarrow in order of output wavelength-span:

MIR-SC fibre design:		<ul style="list-style-type: none"> • SIF, NA=1.0 • core/clad.= AsSe/GeAsSe • core: $\varphi \sim 16 \mu\text{m}$ • 85 mm long 	<ul style="list-style-type: none"> • SIF, NA=1.3 • core/clad.= GeAsSe/GeAsS • core: $\varphi=4.5 \mu\text{m}$ • 110 mm long 	<ul style="list-style-type: none"> • SIF • core/clad. GeSbSe/GeSe • core: $\varphi = 6.0 \mu\text{m}$ • 110 mm long 	<ul style="list-style-type: none"> • 'holey' PCF • air/Ge-As-Se • taper core: $\varphi = 6.7 \mu\text{m}$ • $\sim 60 \text{ cm}$ long 	<ul style="list-style-type: none"> • SIF, NA = 0.3 • core/cladding= 'AsS' • core: $\varphi=10 \mu\text{m}$ • 2 m long 	
INCREASING SC SPAN		\leftarrow					
MIR-SC wavelength span / μm		1.4 to 13.3	1.5 to 11.7	1.8 to 10	2.2 to 12.0	1.0 to 8.0	1.9 to 4.8 #
MIR-SC av. power out / W		'few 100 μW		'few' mW	17 mW	57.3 mW	565 mW
Pump laser:	Pump type	OPA		OPA	OPA	1.04 μm laser + CW seed laser in nonlinear crystal	Raman-shifted Er^{3+} SiO_2 mode-locked fibre
	Centre wavelength / μm	6.3	4.5	4.0	4.485	4.0	2.45
	Pulse width / fs	100		330 ± 15	330	250	-
	Pulse rate / kHz	1		21,000	21,000	21,000	10,000
	Peak power / kW	2290	1250	~ 3	6.9	16	> 3.5
	Av. pump power	$\sim 760 \mu\text{W}$	$\sim 350 \mu\text{W}$	40 mW	66 mW	200 mW	1.4 W
Year [reference]		2014 [28]		2015 [30]	2016 [31]	2017 [32]	2012 [22]

KEY: av = average; clad.=cladding; PCF=photonic crystal fibre; OPA=optical parametric amplifier; φ = diameter; (#) = - 20 dB point.)

MIR quantum cascade lasers (QCLs) are a competing technology for fibre MIR-SC but must be arrayed to provide wideband MIR coverage. In contrast, MIR-SC fibre lasers are broadband, can cover the MIR spectral region, can be brighter than synchrotron-generated MIR light, have good beam quality, are readily integratable with fibre-optics and have already been demonstrated [28, 31].

Taking the SIF (step-index-fibre) MIR-SC with best broadband spectral brightness from 2.2-12 μm now achieved [31] (see Table 1), Fig 8 (compiled in MINERVA) compares existing MIR sources [33]. It can be seen from Fig. 8 that commercial fibre MWIR-SC covering 3-5 μm [34] are as spectrally bright as the longer wavelength quantum cascade lasers [35]. Also compared are the brightness of wideband sources based on the GloBar[®] blackbody radiant source and a synchrotron (SR) generated MIR beam [36]. Fig. 8 demonstrates that fibre MIR-SC lasers have now been realised that are equivalent to the output of several combined synchrotron-generated MIR beams and broadband, but not as bright as an array of MIR-QCLs. To reiterate, the key advantage of fibre MIR-SC over the arrayed MIR-QCLS is that one source covers the wider range.

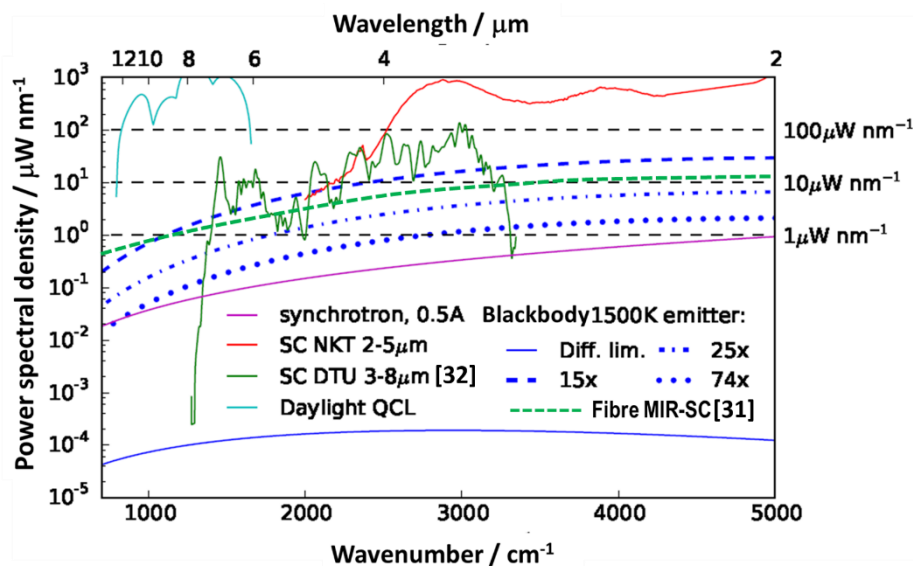


Figure 8. Comparison of spectral brightness of available MIR sources. Compared are: GloBar[®] type of common thermal, blackbody with broadband emission; synchrotron (data take from the Diamond Light Synchrotron webpage - due to Dr Gianfelice Cinque [36]) arrayed quantum cascade lasers (data taken from [35] (note that QCLs down to 3.0 μm are now available); cartoon of the most powerful wideband SIF MIR-SC data to date [31] and a commercial fibre MWIR SC system from [34]. (Redrawn from [33].)

MIR-QCLs exhibit poor beam quality, are not readily integrated with MIR fibre-optics and can only be pulsed on a duty cycle. MIR-QCLs are therefore are not suitable for pumping fibre MIR-SCs. Narrow-line direct-emission fibre lasers, on the other hand, have excellent beam quality, can be pulsed and

are readily integratable with fibre-optics. Record peak power (10.6 kW) at 2.9 μm in an Er^{3+} -ZBLAN fibre laser was achieved in MINERVA [37]. However, MIR fibre lasers but have not yet been demonstrated at $\geq 4 \mu\text{m}$ wavelength [38-41], yet these longer wavelength MIR fibre lasers are needed to pump fibre MIR-SC in order to achieve a compact, wideband, all-fibre MIR-SC system for molecular sensing and imaging.

Progress in RE MIR fibre pump lasers for pumping nonlinear MIR fibre for MIR-SC generation

During MINERVA, for the first time bright, broadband photoluminescence from 3.5 to 6 μm was observed in small-core MIR chalcogenide glass optical fibres with long radiative lifetimes [40]. This is a necessary step in the quest to develop long wavelength, narrow band MIR fibre lasers for pumping fibre MIR-SC broadband lasers for an all-fibre system.

Progress in passive fibre for routeing

Also during MINERVA, record low optical loss of 80 dB / km at 6.6 μm was reported in passive fibre for routeing MIR light [42] with MIR passive light transmission through 83 m fibre . This result complements other similar low optical loss results for other chalcogenide glass compositions reported in the literature over the last few years [see refs. in [42]].

Progress in tissue *ex vivo* imaging using fibre mid-infrared MIR supercontinuum (SC) laser sources

Ex vivo imaging, but not yet *in vivo* imaging, has been carried out very recently using fibre mid-infrared (MIR supercontinuum (SC) lasers as detailed in the following two sub-sections. Thus, Février *et al.* carried out MIR spectroscopic transfection [43] imaging within the 3 μm to 5 μm (3333 cm^{-1} to 2000 cm^{-1}) spectral range. They compared their results to MIR microspectroscopy imaging carried out in a commercial FTIR using a synchrotron (SR) generated MIR light source [43]; in particular signal-to-noise ratios were evaluated and compared.

MINERVA has reported the first demonstration of fibre MIR-SC imaging beyond 5 μm ($< 2000 \text{ cm}^{-1}$) wavelength and compared the results to those obtained with MIR microspectroscopy imaging carried out in a commercial FTIR using a traditional blackbody source [44].

Fibre MIR-SC laser imaging 3 μm to 5 μm (3333 cm^{-1} to 2000 cm^{-1})

Février *et al.* [43] demonstrated that fibre-based supercontinuum (SC) sources in the mid-infrared (MIR) enable diffraction-limited FTIR spectromicroscopy. A Tm^{3+} -doped silica-glass fibre laser was used to deliver 40 ps pulses at 1952.7 nm which were amplified and used to pump 20 m of a fluoride-glass (ZBLAN) fibre (see Fig. 5) to deliver a fibre MIR-SC which was continuous and relatively flat from 2 μm to $\sim 3.75 \mu\text{m}$ with spectral power density of *ca.* 1 mW nm^{-1} . The Authors modelled the residual coherence using the generalised nonlinear Schrödinger equation, including amplified spontaneous emission noise in the Tm^{3+} -doped fibre amplifier. They calculated the spectrally resolved modulus of the complex degree of mutual coherence, which gave a measure of the phase stability and temporal coherence. The output fibre MIR-SC spectrum exhibited some degree of coherence around the pump wavelength only; it was almost fully incoherent in the vicinity of the C-H vibrational absorption stretching band. A 500 nm wide bandpass, filter centred at 3500 nm, was used to select the C-H vibrational spectral region from the fibre MIR-SC laser output. Under these experimental conditions, the fibre MIR-SC coherence length was $\sim 20 \mu\text{m}$ and this short coherence length made it comparable to that of a thermal blackbody MIR source. The fibre MIR-SC laser beam after filtering was expanded and collimated to approximately 25 mm width and routed into a FTIR spectrometer equipped with a MIR microscope.

The tissue sample was a thin section of human liver extracted using a fine-needle biopsy from a non-alcoholic fatty liver (NAFL) disease patient and was prepared by cryosectioning to 10- μm thickness without embedding in paraffin and mounted on a low-e MIR reflective microscope slide. Spectra were collected from sample in the MIR microscope by means transfection. To limit the power falling on the MCT detector, in order for it to operate in its optimal linearity range, the fibre MIR-SC laser source intensity was actually reduced by two orders of magnitude using a neutral density filter at 3500 nm.

In order to evaluate signal-to-noise ratios (SNR), spectra were measured at 4 cm^{-1} resolution with 256 co-added scans. The root mean square (RMS) noise level was estimated in the 4000–4200 cm^{-1} range, where no specific biomolecular absorption peaks were present, in absorbance units, and the SNR was calculated as the inverse of the RMS noise value.

The MIR spectroscopy imaging performance achieved with the fibre MIR-SC laser source was compared to that achieved with a MIR synchrotron (SR) light source for two small aperture sizes of

$(5 \times 5) \mu\text{m}^2$ and $(3 \times 3) \mu\text{m}^2$. At the $(5 \times 5) \mu\text{m}^2$ aperture size, the fibre MIR-SC laser source exhibited a SNR above 200 in 8 scans; 32 scans of the MIR-SR radiation source were needed to reach the same SNR level. The MIR spectral imaging and selected spectra shown in Fig. 9 and were obtained at the $(3 \times 3) \mu\text{m}^2$ aperture size. Using the fibre MIR-SC laser source [Figs. 9(c) and 9(e)], $\sim 1\%$ RMS (root mean square) noise level was found with 16 co-added scans; the fibre MIR-SC imaging was comparable to that obtained with the MIR-SR source with 128 co-added scans [Figs. 9(b) and 9 (d)], which was an 8 x slower acquisition. To compare the performance of the two sources, the signal-to-noise (SNR) ratio for the fibre MIR-SC laser source and the MIR-SR source *versus* the number of scans at the aperture of $(3 \times 3) \mu\text{m}^2$ are given in the inserts of Figs. 9(d) and 9(e). Figure 9 shows that the fibre MIR-SC laser allows collection of MIR spectroscopic tissue images that match those obtained with the MIR-SR source at diffraction-limited aperture sizes. At this resolution, the Authors conclude that the stability of the fibre MIR-SC laser system is sufficient to obtain SNRs suitable for tissue microspectroscopy.

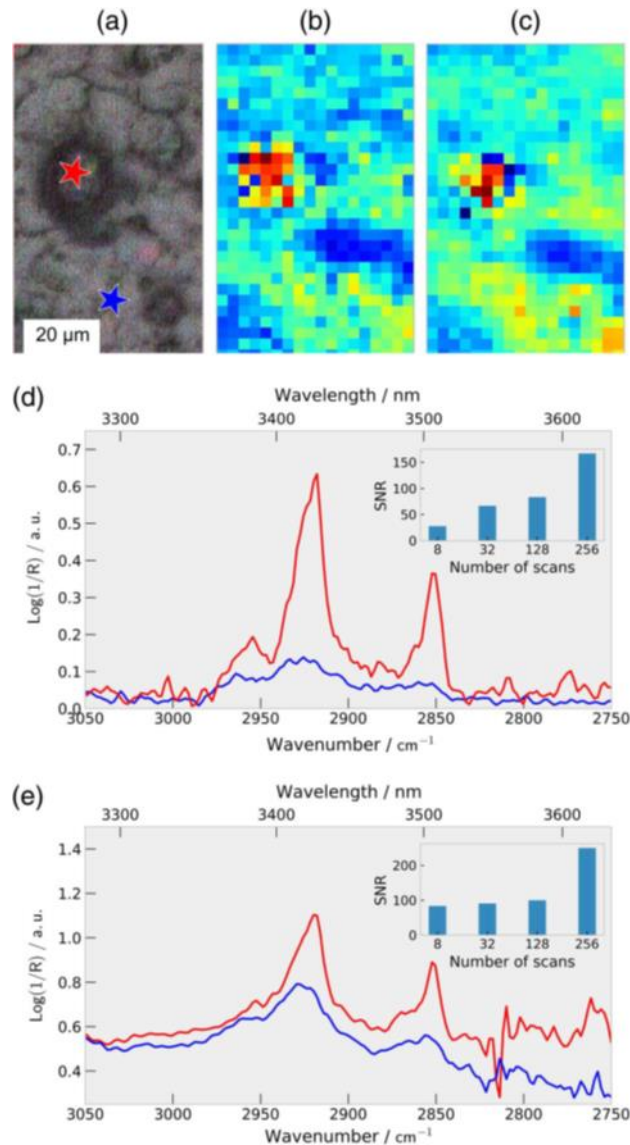


Figure 9. Comparison of MIR spectral imaging recorded with the fibre-based MIR-SC laser source and with the MIR-SR source. The MIR spectroscopic imaging of lipid vesicles in a liver section generated on the ν_{asym} CH_2 absorption of lipids at $3.42 \mu\text{m}$ (2920 cm^{-1}). (a) Optical micrograph of the mapped area. The scale bar indicates $20 \mu\text{m}$ length. (b) MIR spectral tissue image recorded with 128 scans at $(3 \times 3) \mu\text{m}^2$ aperture with the MIR-SR source. (c) MIR spectral tissue image recorded with 16 scans at $(3 \times 3) \mu\text{m}^2$ aperture with the fibre MIR-SC laser source. (d), (e) Spectra of the C-H stretching regions showing CH_3 and CH_2 peaks recorded with (d) the MIR-SR radiation source and (e) the MIR-SC laser source. Blue and red colors on (d), (e) correspond to the positions of the same colour markers on (a). Insets: SNR measured versus the number of scans at the highest resolution of $(3 \times 3) \mu\text{m}^2$. (Reproduced with permission from [43].)

No baseline correction of spectra was carried out. Spectral quality was reached in only 16 scans using the fibre MIR-SC laser source, which was 8 x faster than the measurement performed with the MIR-SR radiation. Spectra recorded with the fibre MIR-SC laser source appear noisier below the 2850 cm^{-1} peak. A slight baseline shift and an apparent decrease of the 2950 cm^{-1} peak was observed when using the fibre MIR-SC laser source. In both the MIR-SR radiation case and the fibre MIR-SC laser case, the red spectral peak heights (Figs. 9(d) and (e)) at $\sim 2925 \text{ cm}^{-1}$, were proportional to concentration but consistently differed between the two sources and these discrepancies were

attributed to the combination of alignment and fibre MIR-SC laser source instability, as well as the small aperture and raster step-size.

As shown in the insets of Figs. 9(d) and (e), the SNR improved on increasing the number of scans. The SNR of the fibre MIR-SC laser source remained *ca.* constant when decreasing the aperture size, whereas the MIR-SR source where SNR for full beam intensity decreased by a factor of 100 on decreasing the aperture size decreases from $(20 \times 20) \mu\text{m}^2$ to $(3 \times 3) \mu\text{m}^2$ due, the Authors suggest, to the higher photon flux passing through this small aperture in the case of the fibre MIR-SC laser source.

In conclusion, the SNR obtainable with the laser source was found to be comparable to, or surpassed, those available with a MIR-SR source in shorter acquisition times even at very small aperture sizes. Such performance at such small aperture size would not be achieved with a traditional, thermal blackbody source, due to its low brightness.

MINERVA fibre MIR-SC laser imaging beyond $5 \mu\text{m}$ (2000 cm^{-1})

The MINERVA Project recently reported the first proof-of-principle demonstration, to best knowledge, of MIR spectral tissue imaging using a fibre MIR-SC laser source within the diagnostically-important, longer wavelength fingerprint region [44].

A chalcogenide-glass fibre MIR-supercontinuum (SC) laser source emitting from 2 to $7.5 \mu\text{m}$ (5000 cm^{-1} to 1333 cm^{-1}) with 25 mW output was used; MIR spectroscopic imaging was carried out at selected wavelengths between 5.7 (1754 cm^{-1}) and $7.3 \mu\text{m}$ (1370 cm^{-1}) by point-scanning in transmission of a sub-mm sample of colon tissue. These wavelengths lie beyond the capabilities of commercially available fluoride-glass fibre MIR-SC lasers (see last sub-section; see Fig.5). The fibre MIR-SC was generated in a tapered large-mode-area chalcogenide-glass photonic crystal fibre (PCF) for bandwidth and high average power. Single-mode output was designed-in for diffraction-limited imaging performance. In the optical set-up, for point-scanning the sample was on a piezo-electric scanning stage. The fibre MIR-SC laser was pumped with a chopped optical parametric amplifier (OPA) laser (250 fs , $4.3 \mu\text{m}$ wavelength). After interaction with the tissue sample, the fibre MIR-SC laser light was routed *via* a passive chalcogenide glass MIR fibre to a grating spectrometer for wavelength selection and detected, with the help of a lock-in amplifier to the chopper frequency, by means of a mercury-cadmium-telluride (MCT) detector.

Note that, during the scan, the fibre MIR-SC laser exposure was about 15 x lower than the maximum permissible exposure level recommended for skin in the IEC 60825-1:2014 International Standard, and no effects due to tissue heating were observed.

The sample was a 7 μm thick non-tumoral colon tissue section which had been formalin-fixed and paraffin-embedded and then mounted on a CaF_2 MIR-transmissive substrate. An adjacent 3 μm tissue section was subjected to 'Gold Standard' haematoxylin and eosin (H&E) staining on a glass slide. The Authors report that the: 'H&E image displayed a typical normal tissue structure consisting of the epithelial glands (colonic crypts) with darkly stained outer nuclear regions, lightly stained inner cytoplasmic regions, connective tissue, thin muscle layer, and mucin secretions' (Fig. 10). The Authors point out that to be useful in pathology, a MIR spectroscopic imaging must be able to identify these histological regions of the tissue based on the molecular features, and most importantly the epithelial regions that are directly associated with cancer development, and the connective tissue. For this reason, the fibre MIR-SC laser imaging was performed at wavelengths characteristic of some key molecular absorption features of the sample tissue, whose absorption band shape and band intensity can be related to cancer *viz.*: amide I, II protein bands ($\sim 6.03, 6.45 \mu\text{m}$, respectively) the lipid ester ($\sim 5.7 \mu\text{m}$) and C-H bending ($\sim 7.3 \mu\text{m}$).

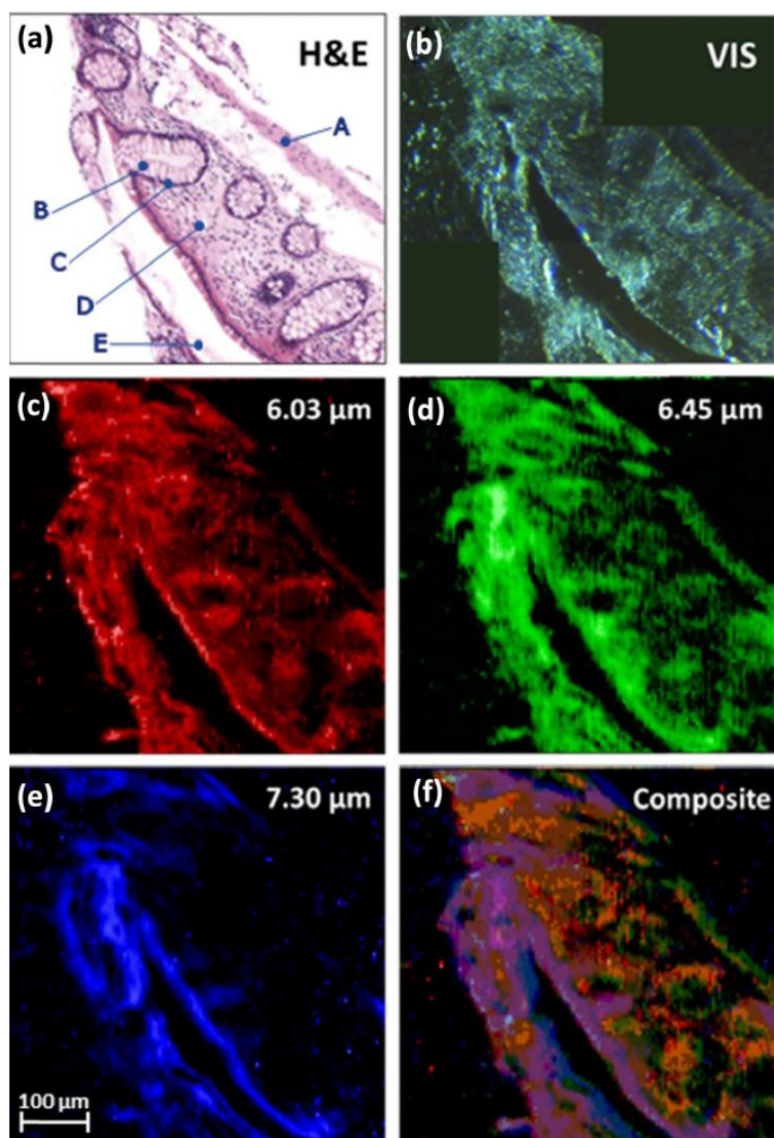


Figure 10. Comparison of: (a) the confocal image of the H&E stained tissue section with identification of the various histological regions: A, muscle layer; B/C, cytoplasmic/nuclear regions of the colonic crypts; D, connective tissue; E, mucin secretions. (b) Visible light transmission image of the un-stained sample. (c), (d) MIR transmission images of the protein rich amide regions highlighting the nuclear regions of the colonic crypts, and (e) the mucin secretions and surface epithelial walls. (f) Composite image showing the spectral-spatial mapping of (c)–(e). (Reproduced with permission from [44].)

The fibre MIR-SC transmission tissue spectroscopic images were compared (Fig. 11) with those obtained from a bench-top FTIR microspectroscopy imaging system with Global[®] blackbody light source and light source, 128 × 128 MCT focal-plane array (FPA) with pixel size of (5.5 × 5.5) μm². This conventional imaging was collected at a spectral resolution of 4 cm⁻¹, averaging over 64 scans; the full hyperspectral cube took 5 min to acquire, plus an additional 15 min to complete 256 background scans. This may be compared with the 24 min acquisition time using the fibre MIR-SC point scanning optical set-up.

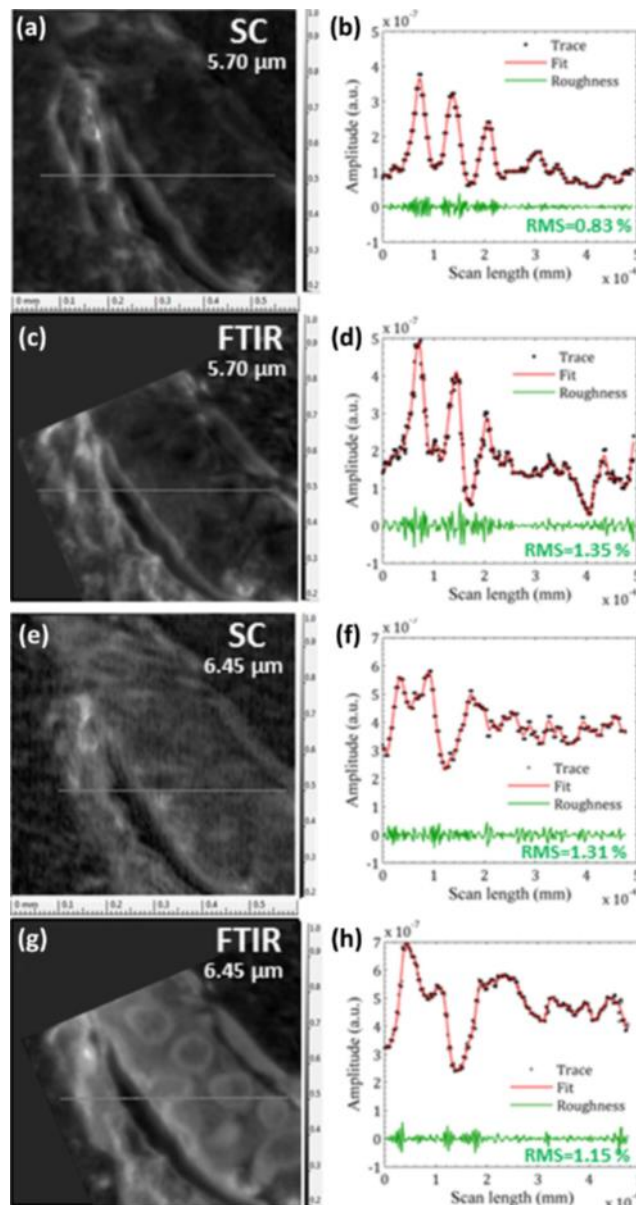


Figure 11. (a), (c), (e), (g) MIR transmission spectroscopic images measured at 5.7 μm and 6.45 μm wavelengths using either the fibre MIR-SC with grating spectrometer or conventional FTIR microspectroscopy with blackbody thermal source. (b), (d), (f), (h) Contrast line traces corresponding to the lines in (a), (c), (e), (g), and spatial noise analysis based on the roughness tool from the visualization and analysis software Gwyddion. (Reproduced with permission from [44].)

The comparison revealed a reduced contrast in the fibre MIR-SC images compared to the thermal source and microspectroscopy in the FTIR. The Authors suggest how to mitigate this but acknowledge that the high spatial coherence of the fibre MIR-SC laser beam may have introduced some differences. The point-scanning system was inherently slower than the FPA imaging.

Conclusions, what was achieved on MINERVA and next steps

To recap, the two applications addressed in MINERVA were: (i) high volume pathology screening *i.e.* automated microscope-based examination of cell and tissue excised biopsy samples, and (ii) *in vivo*, real-time skin surface examination, working towards the MIR optical biopsy.

For (i) – high throughput MIR pathology - the research carried out during MINERVA produced record results of $1\ \mu\text{m}^2$ spatial resolution tissue imaging using conventional FTIR microspectroscopy with a traditional thermal blackbody source. However, it was concluded that this extra data processing does not lead to significantly greater tissue statistical differentiation. Other progress made (topological image registration, biochemical interpretation of tissue MIR spectra) can be found by reading the MINERVA final report, available on the website [45].

For (ii) - the MIR optical biopsy - the MINERVA research produced record results of broadband fibre MIR-SC, record low optical loss passive MIR fibre for transmission and first report of MIR photoluminescence and long PL lifetimes in small core rare earth ion doped MIR fibre for MIR fibre lasing above $4\ \mu\text{m}$ wavelength; these represent steps towards the construction of an all-fibre MIR-SC optical system for *in vivo* tissue MIR imaging. MINERVA research has resulted in the first report of fibre MIR-SC spectroscopic imaging wavelengths in the ‘fingerprint region’ working towards MIR spectral discrimination of disease.

Next steps

What is now required is:

- (i) optimisation of fibre MIR-SC from $2\ \mu\text{m}$ to at least $10\ \mu\text{m}$, and ideally $15\ \mu\text{m}$, wavelength for low temporal coherence (as indicated by the work of Février *et al.* [43]) and low noise in step-index fibre;
- (ii) realisation of narrow-line direct emission MIR fibre lasers for pulsed operation in the $4\ \mu\text{m}$ to $6.5\ \mu\text{m}$ output range for all-fibre pumping of the fibre MIR-SC lasers for compact systems;

- (iii) fast MIR spectral imaging acquisition in a custom-made IR spectrometer to accommodate small spatially coherent MIR optical beams, as opposed to the beam expansion demanded by the interferometer operation of current FTIR designs, whilst maintaining compatibility of the period of the FTIR interferometer with the pulse period of the fibre MIR-SC laser beam;
- (iv) addressing the optimum power for fibre MIR-SC tissue imaging *in vivo* for best spectral resolution without tissue degradation together with numerical and other removal of water in aqueous tissue and live cells;
- (v) sensor head design including optimal endoscopy design for either *in vivo* reflectance or ATR (attenuated total reflection) of tissue with hermetic packaging, use of diamond and fluoride windows and to be sterilisable;
- (vi) MCT-FPA (mercury-cadmium-telluride focal plane array) detectors available to longer wavelengths and to tolerate higher power-density of signal at the detector, and
- (vii) determination of the 'sweet-spot' of greatest tolerable fibre MIR-SC brightness to give best imaging without tissue damage.

Acknowledgements: the Authors acknowledge funding from the EU FP7 programme for MINERVA. The Authors would sincerely like to thank the following Researchers for their valuable and original scientific and engineering input into the work presented here and within the MINERVA Project: Christian R. Petersen (Technical University of Denmark); Jayakrupakar Nallala (University of Exeter, UK); Gavin R Lloyd of Gloucester Hospital UK (now at University of Birmingham, UK); Jon Ward and Nikola Prtljaga (Gooch & Housego, UK); Cestmir Barta and Radek Hasal (4-BBT Material Processing , Czech Republic); Björn Kemper, Christina Rommel, Juergen Schnekenburger (University of Münster, Germany) Francisco Peñaranda and Valery Naranjo (University of Valencia, Spain) and Slawek Sujecki, Trevor Benson, David Furniss and Zhuoqi Tang (University of Nottingham, UK).

References

- 1 A. B. Seddon, Int. J. Appl. Glass Sci., 2011, 2(3) 177-191.
- 2 M. Diem, S. Boydston-White and L. Chiriboga, Appl. Spect., 1999, 5(4) 148A-161A.
- 3 M. Jackson, M. G. Sowa and H. H. Mantsch Biophys. Chem., 1997, 68(1-3) 109-125.

- 4 L. M. McIntosh, M. Jackson, H. H. Mantsch, M. F. Stranc, D. Pilavdzic, and A. N. Crowson, *J. Invest. Dermatol.*, 1999, 112, 951–956.
- 5 T. P. Wrobel and R. Bhargava, *Anal. Chem.*, 2018, 90 1444-1463.
- 6 G. Bellisola and C. Sorio, *Am. J. Cancer Res.*, 2012 2(1) 1-21.
- 7 C. Krafft, G. Steiner, C. Beleites and R. Salzer, *J. Biophoton.*, 2009 2(1–2) 13–28.
- 8 C. Kendall, M. Isabelle, F. Bazant-Hegemark, J. Hutchings, L. Orr, J. Babrah, R. Baker and N. Stone, *Analyst*, 2009, 134 1029-1045.
- 9 M. Diem, A. Mazur, K. Lenau, J. Schubert, B. Bird, M. Miljkovic, C. Krafft and J. Popp, *Biophoton.* 2013, 6(11-12) 855–886.
- 10 M. J. Baker, J. Trevisan, P. Bassan, R. Bhargava, H. J. Butler, K. M. Dorling, P. R. Fielden, S. W. Fogarty, N. J. Fullwood, K. A. Heys, C. Hughes, P. Lasch, P. L. Martin-Hirsch, B. Obinaju, G. D. Sockalingum, J. Sulé-Suso, R. J. Strong, M. J. Walsh, B. R. Wood, P. Gardner and F. L. Martin, *Nat. Protoc.*, 2014, 9 1771–1791.
- 11 J. Nallala, O. Piot, M-D. le Diebold, C. Gobinet, O. Bouche, M. Manfait, G. D. Sockalingum *Cytometry Part A*, 2013 83A 294-300.
- 12 J. Nallala, G. R. Lloyd, N. Shepherd and N. Stone, *Analyst*, 2016, 141 630-639.
- 13 J. Nallala, G. R. Lloyd and N. Stone, *Analyst*, 2015, 140(7) 2369-2375.
- 14 A. B. Seddon. *Biomedical Applications in Probing Deep Tissue using Mid-Infrared (MIR) Supercontinuum Optical Biopsy in Deep Imaging in Tissue and Tissue-Like Media with Linear and Nonlinear Optics*], eds. R. R. Alfano and L. Shi, Pan Stanford Publishing, Singapore, printed in GB. 2017.
- 15 A. B. Seddon, *J. Non-Cryst. Solids*, 1995 184 44-50.
- 16 P. W. France, M. G. Drexhage, J. M. Parker, M. W. Moore, S. F. Carter and J. V. Wright: *Fluoride Glass Optical Fibres* (Blackie, London 1990).
- 17 BSI ISO 20473:2007 Optics and photonics. Spectral bands. 2007, checked 2015, BSI. p. 10. (British Standards Institution (BSI) and International Organization for Standardisation (ISO).) Consulted September 2016.
- 18 J. S. Sanghera, L. B. Shaw, L. E. Busse, V. Q. Nguyen, P. C. Pureza, B. C. Cole, B. B. Harbison, I. D. Aggarwal, R. Mossadegh, F. Kung, D. Talley, D. Roselle and R. Miklos, *Fibre Integr. Opt.*, 2000 19(3) 251–274.
- 19 R. R. Alfano and S. L. Shapiro, *Phys. Rev. Lett.*, 1970 24 584-587.
- 20 P. St. J. Russell, *Lightwave Technol.*, 2006 24(12) 4729-4749.

- 21 A. Zackery and S. R. Elliott: Optical Nonlinearities in Chalcogenide Glasses and their Applications (Springer Series in Optical Sciences 135, New York, USA, 2007).
- 22 R. R. Gattass, B. L. Shaw, V. Q. Nguyen, P. C. Pureza, I. D. Aggarwal and J. S. Sanghera, *Optical Fibre Tech.*, 2012, 18 345-348.
- 23 Personal communication from J.S. Sanghera (2006).
- 24 J-P. Guin, T. Rouxel and J-C. Sangleboeuf, *J. Am. Ceram. Soc.*, 2002, 85(6) 1545-52.
25. P. Toupin, L. Brilland, D. Méchin, J-L. Adam and J. Troles, *J. Lightwave Tech.*, 2014 32(13) 2428-2432.
- 26 C. Agger, I. Kubat, U. Møller, P.M. Moselund, C.R. Petersen, B. Napier, A.B. Seddon, S. Sujecki, T.M. Benson, M. Farries, J. Ward, S. Lamrini, K. Scholle, P. Fuhrberg and O. Bang: Numerical demonstration of 3-12 μm supercontinuum generation in large-core step-index chalcogenide fibres pumped at 4.5 μm , *Nonlinear Optics 2013, Hawaii, USA, 21–26 July 2013*, ISBN: 978-1-55752-977-0, paper NW4A.09, doi:10.1364/NLO.2013.NW4A.09, *Nonlinear Optics, OSA Technical Digest (online) Optical Society of America 2013*).
- 27H. G. Dantanarayana, N. M. Moneim, Z. Q. Tang, L. Sojka, S. Sujecki, D. Furniss, A. B. Seddon, I. Kubat. O. Bang and T. M. Benson, *Opt. Mater. Express*, 2014, 4 1444–1455.
- 28 C. R. Petersen, U. Møller, I. Kubat, B. Zhou, S. Dupont, J. Ramsay, T. M. Benson, S. Sujecki, N. Abdel-Moneim, Z. Tang, D. Furniss, A. Seddon and O. Bang, 2014, *Nature Photon*, 2014 830-834.
- 29 Gr. Steinmeyer and J. S. Skibina, 2014, *Nature Photonics, News and Views*, 8, 814-815, on impact of work in ref. [28] by Petersen et al..
- 30 Y. Yu, B. Zhang, X. Gai, C. Zhai, S. Qi, W. Guo, Z. Yang, R. Wang, D.Y. Choi, S. Madden and B. Luther-Davies, *Opt. Lett.* 2015, 40(6) 1081-1084.
- 31 B. Zhang, Y. Yu, C. Zhai, S. Qi, Y. Wang, A. Yang, X. Gai, R. Wang, Z. Yang and B. Luther-Davies, *J. Am. Ceram. Soc.*, 2016, 99(8) 2565-2568.
- 32 C. R. Petersen, R. D. Engelsholm, C. Markos, L. Brilland, C. Caillaud, J. Trolès, and O. Bang, *Opt. Exp.*, 2017, 25(13) 15336-15348.
33. I. D. Lindsay, S. Valle, J. Ward, G. Stevens, M. Farries, L. Huot, C. Brooks, P. M. Moselund, R. M. Vinella, M. Abdalla, D. de Gaspari, R. M. von Wurtemberg, S. Smuk, H. Martin, J. Nallala, N. Stone, C. Barta, R. Hasal, U. Moller, O. Bang, S. Sujecki and A. B. Seddon, 2016, *SPIE BiOs, California, USA, Proc. Vol. 9703, Optical Biopsy XIV: Towards Real-Time Spectroscopic Imaging and Diagnosis*, 970304 <https://doi.org/10.1117/12.2210836>.
- 34 www.nktpotonics.com (Accessed September 2016.)
- 35 (a) C. Kumar N. Patel *at* www.pranalytica.com and (b) www.daylightsolutions.com (Both accessed September 2016.)
36. www.diamond.ac.uk Dr Gianfelice Cinque, MIRIAM beamline B22. (Accessed September 2016.)
- 37 S. Lamrini, K. Scholle, M. Schäfer, J. Ward, M. Francis, M. Farries, S. Sujecki, T. Benson, A. Seddon, A. Oladeji, B. Napier, and P. Fuhrberg, *CLEO Europe 2015, European Conference on Lasers and*

Electro-Optics – European Quantum Electronics Conference, 21-25 Jun-2015; Munich, Germany.
ISBN: 978-1-4673-7475-0; paper CJ-7.2, (OSA 2015).

38. J. Schneider, *Elect. Lett.*, 1995, 31(15) 1250-1251.

39. A.B. Seddon, Z. Tang, D. Furniss, S. Sujecki and T.M. Benson, *Opt. Express*, 2010 18(25) 26704-26719.

40 Z. Tang, D. Furniss, M. Fay, H. Sakr, Ł. Sójka, N. Neate, N. Weston, S. Sujecki, T.M. Benson and A.B. Seddon, *Opt. Mat. Exp.*, 2015, 5(4) 870-886.

41 L. Sojka, Z. Tang, D. Furniss, H. Sakr, Y. Fang, E. Beres-Pawlik, T.M. Benson, A.B. Seddon and S. Sujecki, *J. Opt. Soc. America B*, 2017, 34(3) A70-A79.

42 Z. Tang, V. S. Shiryaev, D. Furniss, L. Sojka, S. Sujecki, T. M. Benson, A. B. Seddon and M. F. Churbanov, 2015, 5(8) *Opt. Mat. Exp.* 1722-1737.

43 F. Borondics, M. Jossent, C. Sandt, L. Lavoute, D. Gaponov, A. Hideur, P. Dumas and S. Février, *Optica*, 2018, 5(4) 378-381.

44 C. R. Petersen, N. Prtljaga, M. Farries, J. Ward, B. Napier, G. R. Lloyd, J. Nallala, N. Stone and O. Bang, *Opt. Lett.*, 2018, 43(5) 999-1002.

45 <http://minerva-project.eu> (European funded FP7 Project: acronym: MINERVA, titled: " **Mid- to NEaR** infrared spectroscopy for improVed medical diAgnostics ", (Grant agreement no.: 317803, 2012-2017).